Published in final edited form as:
Biochemistry. 2012 October 30; 51(43): 8491–8501. doi:10.1021/bi3010335.

Effect of β,γ-CHF and β,γ-CHCl dGTP halogen atom stereochemistry on the transition state of DNA polymerase β[†]

Keriann Oertell[‡], **Yue Wu**[‡], **Valeria M. Zakharova**[‡], **Boris A. Kashemirov**[‡], **David D. Shock**[§], **William A. Beard**[§], **Samuel H. Wilson**[§], **Charles E. McKenna**[‡], and **Myron F. Goodman**[‡,┤,*]

[‡]Department of Chemistry, University of Southern California, Los Angeles, California 90089.

[§]Laboratory of Structural Biology, NIEHS, National Institutes of Health, Research Triangle Park, North Carolina 27709.

[┤]Department of Biological Sciences, University of Southern California, Los Angeles, California 90089.

Abstract

Recently, we synthesized the first individual β,γ-CHX dGTP diastereomers ((*R*)- or (*S*)-CHX; X = F or Cl), and determined their structures in ternary complexes with pol β. We now report stereospecificity by pol β on the mixed β,γ-CHX diastereomer pairs using NMR and on the separate diastereomers using transient kinetics. For both the F and Cl diastereomers, the *R* isomer is favored over the *S* isomer for G•C correct incorporation, with stereospecificities [$(k_{pol}/K_d)_R$/$(k_{pol}/K_d)_S$] of 3.8 and 6.3 respectively and also for G•T misincorporation, with stereospecificities of 11 and 7.8 respectively. Stereopreference for the (*R*)-CHF dGTP diastereomer was abolished for k_{pol} but not K_d with mutant pol β (R183A). These compounds constitute a new class of stereochemical probes for active site interactions involving halogen atoms. As Arg183 is unique in family X pols, design of CXY deoxyribonucleotide analogues to enhance interaction is a possible strategy to inhibit BER selectively in cancer cells.

DNA polymerase β (pol β) is essential for single-nucleotide base excision repair (BER), the predominant BER pathway in humans.(1, 2) This small (39 kDa) polymerase has an intrinsic lyase activity, but lacks a proofreading 3′-exonuclease. Excessive levels of pol β are found in a variety of cancers(3), and variants of pol β have been identified in as many as 30% of malignant tumors.(4-12) X-ray crystallographic studies of ternary dNTP/DNA/pol β complexes have revealed the presence of an arginine residue (Arg183) in proximity to the triphosphate β,γ-bridging oxygen of dNTPs bound in the active site of the enzyme. This residue has no counterpart in the replicative DNA polymerases, e.g., cellular pols δ and ε, and mitochondrial pol γ, and thus is a plausible target in the creation of selective inhibitors of pol β that might have relevance to drug design. Pol β has emerged as a potential target for

[†]This research was supported, in part, by the National Cancer Institute of the National Institutes of Health via Grant 5-U19-CA105010, by that National Institutes of Health via Grant R01-GM21422 (to M.F.G.) and by Research Project Numbers Z01-ES050158 and Z01-ES050159 from the Intramural Research Program of the National Institutes of Health, National Institute of Environmental Health Sciences.

[*]To whom correspondence should be addressed. Telephone: (213) 740-5190. Fax: (213) 740-8631. mgoodman@usc.edu.

Competing Financial Interests
The authors declare no competing financial interests.

Supporting Information Available. ^{31}P NMR spectrum of CHF reactions (Fig. S1), ^{31}P NMR of P_β from CHCl reactions (Fig. S2), and a detailed description of the relative use calculation from the NMR experiments. This material is available free of charge via the Internet at http://pubs.acs.org.

combination chemotherapy with PARP inhibitors.(13, 14) It is thus important to evolve structure-based approaches toward pol β probe/inhibitor development.

We previously synthesized a series of dNTP analogues in which the β,γ-bridging oxygen is replaced with substituted methylene groups as probes of pol β active site structure and function. β,γ-dNTP analogues have been used to assess the influence of leaving-group electrostatic charge and structure on the transition state for pol β, providing evidence for chemistry in the rate-determining step during turnover.(15, 16) High-resolution crystal structures of pol β bound to single-nucleotide gapped DNA substrate incubated with a ~50:50 mixture of dGTP β,γ-substituted CXF diastereomers, where X = H, Cl, or CH_3 detected only one isomer, which in each case had the fluorine atom pointing towards the Arg183 residue.(17, 18) In contrast, similar crystal structures of ternary complexes formed from β,γ-substituted CHCl-dGTP showed approximately equal occupancies for both isomeric forms in the active site of pol β.(17, 18)

These observations pose several interesting questions. First, since a chemical reaction in the crystallized complex is difficult to follow kinetically, it would be useful to know whether a similar stereospecificity also occurs in free solution under presteady state conditions, and if so, whether it is manifested in k_{pol} (transition state effect), K_d (ground state effect), or both. Second, in the case of the CXF isomer that was not detected in the active site by crystallography (i.e., *S*-CHF), it is important to establish whether the enzyme can use this isomer in the absence of the competing, preferred *R*-isomer, and if so, its relative rate of incorporation.

To address these questions, it was essential to have at our disposal the previously unknown individual CHF-and CHCl-dGTP diastereomers, to know their absolute configurations (preferably bound into the active site complex of the enzyme), and to elaborate a method to analyze them together or separately in solution during or after enzyme assays. The polymerase incorporation assays alone are inadequate because both the extended DNA and pCHXp (bisphosphonate, standing in for pyrophosphate from normal dNTPs) products from CHX diastereomer pairs are identical. The first examples of individual stereoisomers in this type of nucleotide analogue were recently prepared.(19) The four CHX (X = F, Cl) diastereomers described in this work were demonstrated to exhibit discrete ^{19}F and ^{31}P NMR spectra, allowing them to be distinguished unambiguously in solution, and all four gave single-ligand X-ray crystal structures with pol β, defining their absolute configurations in addition to their specific conformations within the active site, which proved to be very similar.(19) Thus all the necessary tools were now at hand to determine whether the halogen substitution stereochemistry has any effect on binding (K_d), or the transition state (k_{pol}).

We first applied ^{19}F and ^{31}P NMR analysis(19) to determine the relative concentrations of unreacted (*R*)- and (*S*)-β,γ-CHF-dGTP in substrate diastereomer mixtures remaining in solution after some amount of pol β-catalyzed incorporation had occurred. The availability of the individual stereoisomers then allowed us to perform independent transient-state kinetic analyses to explore stereospecificity for correct incorporation opposite template C and misincorporation opposite T for the CHF- and CHCl-dGTP analogues. By comparing the wild type (wt) pol β incorporation kinetics for the individual diastereomers with a mutant pol β where Arg183 is replaced by alanine (R183A), we could also examine whether a specific electrostatic interaction between Arg183 and the fluorine atom is implicated in any observed stereospecificity for the *R*-isomer, which is relevant to assessing the potential of Arg183 as an element in future design of selective pol β inhibitors.

Materials and Methods

DNA synthesis, purification, radiolabeling, and annealing

Primer (5′-TAT TAC CGC GCT GAT GCG C), template, (5′-GCG TTG TTC CGA CCC CCC GCG CAT CAG CGC GGT AAT A for NMR experiments, or 5′-GCG TTG TTC CGA CMG CGC ATC AGC GCG GTA ATA, M = C or T for transient-state assays), and 5′-phosphorylated downstream (5′-GTC GGA ACA ACG C) oligomers were synthesized on a solid phase DNA synthesizer and purified by 16% denaturing polyacrylamide gel electrophoresis, followed by desalting using oligonucleotide purification cartridges. For the NMR analysis, 1 mol equiv primer was mixed with 1.2 mol equiv template, heated to 95 °C and cooled slowly to room temperature to anneal the strands. For transient-state kinetic assays, 1 mol equiv primer was 5′-end labeled with 0.4 U/μL T4 polynucleotide kinase and 0.7 mol equiv [γ-^{32}P]ATP with the supplied buffer at 37 °C for 30 minutes, followed by heat inactivation at 95 °C for 10 minutes. The primer was purified by size exclusion chromatography using a Bio-Spin 6 column, then annealed by mixing with 1.2 mol equiv template and 1.5 mol equiv downstream oligomers. The mixture was heated to 95 °C and cooled slowly to room temperature.

Protein, reaction buffer, and dGTP-β,γ-CHX preparation

Wild-type and R183A mutant pol β were purified as previously reported.(20) The reaction buffer for all experiments consisted of 50 mM Tris-Cl, 20 mM KCl, 20 mM NaCl, 10 mM $MgCl_2$, 1 mM DTT, and 6% glycerol at pH 8.0, 37 °C. Analogues (*R*/*S*)-β,γ-CHX-dGTP (X = F – 1a/b; X = Cl – 4a/b) were synthesized according to literature procedures.(16, 18, 19)

NMR assay

Nine individual reaction tubes (100 μL final volume in each) containing 50 μM unlabeled and annealed primer/template were incubated with 100 μM wt pol β (final concentrations) in reaction buffer for 3 minutes at 37 °C, followed by addition of (*R*/*S*)-β,γ-CHF-dGTP to a final concentration of 1 mM (500 μM of each diastereomer). The reactions were allowed to proceed for 5 h to incorporate up to 6 consecutive correct nt, followed by heating to 95 °C for ten minutes to melt the DNA. The reaction mixtures were pooled and centrifuged using a Microcon YM-3 column to exclude any reactants or products >3 kDa. The pH of all NMR samples was adjusted to 9.8 – 10.0 with Na_2CO_3 and trace divalent metal ions were removed with Chelex®-100. The resulting reaction mixture, 500 μL was then loaded into an NMR tube following insertion of a coaxial insert containing D_2O as an external reference. NMR spectra of compounds 1a/b before incorporation by pol β were obtained in D_2O with a net concentration of 10 mM. Spectra of the assay samples were obtained using external D_2O reference, with a net concentration of the two diastereomers of ~0.7 mM. The (*R*/*S*)-β,γ-CHCl-dGTP reactions were carried out in an identical fashion with the exception of reaction time, which was 8 h. Wilmad® coaxial insert (stem L 50 mm) was purchased from Sigma Aldrich. ^{19}F and ^{31}P NMR spectra were obtained on Varian 400-MR 2-Channel NMR Spectrometer. All chemical shifts are given on the δ–scale in parts per million (ppm) relative to external 85% H_3PO_4 (δ 0.00, ^{31}P NMR) and $CFCl_3$ (δ 0.00, ^{19}F NMR). ^{31}P NMR spectra were proton-decoupled. The signals of (*R*)-β,γ-CHF-dGTP and (*S*)-β,γ-CHF-dGTP diastereomers on ^{19}F and ^{31}P NMR spectra were assigned according to McKenna *et al.*(19)

NMR settings

^{19}F NMR of dGTP-β,γ-CHF (1a/b) before incorporation by pol β was acquired using Varian 400-MR default setting with 75188 Hz sweep width and -67773 Hz offset. ^{31}P NMRs of dGTP-β,γ-CHF (1a/b) and dGTP-β,γ-CHCl (4a/b) before incorporation by pol β were acquired using Varian 400-MR default setting with 4882 Hz sweep width, 109 Hz

offset and 0.30 Hz/point digital resolution. ^{19}F NMR of the assay sample was acquired using 4.600 μsec pulse width, 1.0 sec relaxation delay, 1.59 Hz/point digital resolution, 52038 Hz sweep width, - 81878 Hz offset, 0.63 sec acquisition time and 26000 number of acquisition. ^{31}P NMR of the assay samples were acquired using 4.650 μsec pulse width, 1.0 sec relaxation delay, 0.30 Hz/point digital resolution, 4882 Hz sweep width, 109 Hz offset, 3.36 sec acquisition time and 12000 number of acquisition.

Transient-state kinetic analyses

Radiolabeled single-nucleotide gapped DNA (100 nM) was incubated with 600 nM pol β in reaction buffer (2x mixture) for 3 minutes at 37 °C. Equal volumes of the DNA/pol β mixture and a 2x solution of (*R*)-β,γ-CHX-dGTP or (*S*)-β,γ-CHX-dGTP at different concentrations were rapidly combined using a KinTek model RQF-3 quench flow apparatus. After the appropriate reaction time, the reaction was quenched with 0.5 M EDTA (pH 8.0). Reaction times longer than 20 seconds were mixed by hand. Reaction products were separated by 20% denaturing polyacrylamide gel electrophoresis (39 cm × 33 cm × 0.4 mm). Dehydrated gels were exposed to a phosphor screen and detected by phosphorescence emission. All reactions were carried out in triplicate.

Results

Preferential insertion of (R)-CHF dGTP from a ~1:1 mixture of the R- and S-diastereomers

Deoxyribonucleotide insertion by pol β was determined by measuring the amounts of unreacted (*R*)- and (*S*)-CHF dGTP remaining after the large-scale reaction had been terminated following the incorporation of up to 6 consecutive nt. Figure 1 shows ^{19}F NMR spectra of a reaction mixture consisting of DNA, wt pol β, and the *R*- and *S*-diastereomers of β,γ-CHF-dGTP present in approximately equimolar starting concentrations. The ^{19}F NMR spectra were taken before and after a 5 h reaction with pol β as an offset overlay, with time zero (pink) above the reaction spectrum (blue). The same mixtures were used to obtain ^{31}P NMR spectra (Fig. S1), yielding data that are consistent with the ^{19}F NMR analysis. Figure 1B, which shows the entire region of interest in the ^{19}F spectrum, allows calculation of the reaction progress based on the amount of fluoromethylenebisphosphonate (pCHFp) product observed relative to the amount of unreacted β,γ-CHF-dGTP remaining (peaks 3 and 1a,b respectively). Focusing on the remaining unreacted triphosphate analogue (Fig. 1C), it is apparent that the two distal peaks can be assigned to individual diastereomers. The outside peak to the left is assigned to (*S*)-β,γ-CHF-dGTP and that to the right is assigned to (*R*)-β,γ-CHF-dGTP.(19)

After a 5 h incubation with primer/template DNA and pol β, the amount of β,γ-CHF-dGTP incorporated corresponds to nearly 30% utilization of the analogue, as revealed by integration of the bisphosphonate and nucleotide peaks in the ^{19}F NMR spectrum. From the ^{31}P NMR (Fig. S1), only 1.5% of the triphosphate analogue was converted to dGMP and bisphosphonate by a degradation process, as opposed to being incorporated into the DNA by pol β. Integration of the bisphosphonate and nucleotide peaks (Fig. 1C) before and after reaction shows that both diastereomers must have been used, in order to account for the amount of bisphosphonate product formed and that the relative consumption of isomers during the reaction was 3:1 (*R*:*S*) (see Supplementary Information for a detailed description of the calculation). This experiment shows unequivocally that (*S*)-β,γ-CHF-dGTP is also a substrate of pol β under these mixed stereoisomer conditions, despite not being detected(17, 18) in a ternary complex structure by X-ray crystallographic analysis, formed by exposure of binary DNA pol β-ddCTP-DNA crystals to solutions of the mixed stereoisomers.

Kinetics of individual (R)- and (S)-β,γ-CHF-dGTP diastereomer utilization

The DNA incorporation reactions of the individual (*R*)- and (*S*)-β,γ-CHF-dGTP diastereomers catalyzed by pol β were analyzed using quench-flow transient-state kinetic assays. For each diastereomer, exponential time courses with different analogue concentrations were determined to measure correct incorporation opposite dC (Fig. 2A) and misincorporation opposite dT (Fig. 2B). The percentage of primer extended is shown plotted versus time, and the data for each concentration is fit to the first order exponential $y = a(1-e^{-kt})$, where a is the maximum percent of primer extension and k is the observed rate constant. The observed rate constant (k_{obs}) is plotted versus the corresponding analogue concentration, and the data fit to the rectangular hyperbola $k_{obs} = k_{pol}[\beta,\gamma\text{-CHF-dGTP}]/(K_d + [\beta,\gamma\text{-CHF-dGTP}])$ to give the k_{pol} and K_d parameters (Fig. 2, Table 1). The stereospecificity (S) is given by the k_{pol}/K_d ratios for the stereoisomers; $S = (k_{pol}/K_d)_R/(k_{pol}/K_d)_S$ (Table 1). Both dGTP diastereomers were incorporated opposite dC in the single-nucleotide gapped DNA substrate, visualized as the addition of a single deoxynucleotide to the 3′-end of the primer strand (Fig. 2A, P+1 PAGE band). The *R* diastereomer was incorporated with a 2-fold larger k_{pol} and a 1.5-fold smaller apparent K_d than the *S*-diastereomer, resulting in S = 3.8 (Table 1), which agrees with S = 3 as obtained by NMR, within the estimated error. The agreement between the NMR and kinetic methods indicates that DNA polymerase substrate specificity measured with two dNTPs competing directly for incorporation into DNA, is equivalent to using kinetics to determine specificity by measuring k_{pol}/K_d values for dNTP substrates in separate reactions(21) and is in accord with a model by Fersht.(22)

Elevated concentrations of (*R*)- and (*S*)-β,γ-CHF-dGTP substrates (125 to 2,000 μM) were used to measure misincorporation opposite template T (Figure 2B, P + 1, P + 2 PAGE bands). The formation of mispairs opposite T show a much larger disparity between the catalytic rates for the *R* and *S* diastereomers ($k_{pol,R}/k_{pol,S} \sim 14.4$), than observed for incorporation opposite C ($k_{pol,R}/k_{pol,S} \sim 2.0$), whereas the overall apparent binding constants were similar (i.e., within a factor of 2), for incorporations opposite either C or T (Fig. 2, Table 1). The P+2 gel band (Fig. 2B, left hand gel) represents a correct incorporation opposite the downstream C occurring via strand displacement at the high substrate concentrations required to detect misincorporation.

The (*S*)-β,γ-CHF-dGTP “missing” from the ternary crystal structure obtained using the diastereomer mix(17, 18) was observed in the crystal structure using the individual *S*-diastereomer alone.(19) The ternary crystal structure obtained with the individual *R*-isomer showed it in the same active site location found using the *R* and *S* mixture, with the fluorine atom pointed towards Arg183.(17, 18) The new structure containing the *S*-diastereomer was observed to overlay closely with the *R*-diastereomer, but with F pointing away from Arg183. The F atom in the *R*-diastereomer was 3.1 Å from a nitrogen atom of Arg183, suggesting the possibility of an F-guanidinium (Arg183) electrostatic interaction.

High-resolution ternary complex structures with pol β bound to single-nucleotide gapped DNA in the presence of β,γ-substituted-dGTP analogues CHCl, CHBr, and CHMe, contained both *R*- and *S*-diastereomers in about equal amounts. In contrast, the structures obtained using β,γ-CXF-dGTP analogues contained the *R*-diastereomer.(17) Increased stability afforded by F atoms in the *R*-configuration interacting with Arg183 in pol β might favor crystal complex formation vs. the *S*-diastereomer. When both diastereomers are present, the selectivity need be only ~3,(17, 18) consistent with the small K_d effects seen in solution.

Preferential insertion of (R)-CHCl over (S)-CHCl dGTP from a diastereomeric mix by pol β

Figure 3 shows the ^{31}P NMR of a reaction mixture consisting of p/t DNA, pol β, and (*R/S*)-β,γ-CHCl-dGTP where the *R*- and *S*-diastereomers are present in equimolar starting concentrations. The upper (pink) spectrum was obtained before the reaction, and the lower (blue) spectrum was the same mixture after an 8 h incubation at 37°C. Reaction progress was determined by dividing the integral of the bisphosphonate peak at ~13 ppm (compound 5, and labeled as such on spectra) by two, due to the two P atoms in the bisphosphonate molecule, and is calculated to be 27% (Fig. 3B). From the observation of P_α resonances (Fig. 3C), the relative consumption of the *R*- and *S*-diastereomers can be calculated the leftmost peak is attributed solely to the *S*-diastereomer, and the rightmost one solely the to the *R*-diastereomer, as discussed above. The diastereomers consumed during the reaction in a ratio of 7:1 (*R*:*S*). See Figure S2 for a zoom in of the P_β signals which yield the same result. About 3% of the initial analogue in the reaction mixture was decomposed into dGMP and chloromethylenebisphosphonate, pCHClp, (Fig. 3B, compound and peak 2).

Presteady state kinetics with separated (R)-CHCl and (S)-CHCl diastereomers

The individual (*R*)- and (*S*)-β,γ-CHCl-dGTP diastereomers were used as substrates in presteady state assays with pol β (Fig. 4). As with the fluorine analogues, time courses were carried out at six concentrations of each substrate for correct incorporation opposite dC (Fig. 4A) and misincorporation opposite dT (Fig. 4B). The data were plotted and analyzed in the same way as with the fluorine analogues. The values of k_{pol} and K_d are given in Table 1.

As observed in the NMR experiment, both diastereomers are incorporated by pol β, however the diastereomer with the chlorine atom oriented towards the R183 residue (*R*) is incorporated with a slight catalytic advantage (7.6 s^{-1} vs. 4.8 s^{-1}) and an apparent binding constant ~ 3-fold lower than the *S* diastereomer (3.2 μM and 11 μM respectively, Table 1). The stereospecificity ratio $[(k_{pol}/K_d)_R/(k_{pol}/K_d)_S]$ S = 6.3 is in agreement with S = 7 obtained using the NMR method. Therefore, the observed relative incorporation of (*R*)-CHCl over (*S*)-CHCl is slightly larger than the approximate detection limit for distribution of each diastereomer in the tertiary crystal structure, which showed equal populations of (*R*)-CHCl and (*S*)-CHCl.(17)

Kinetic analysis of stereoisomeric substrates with the R183A mutant of pol β

To examine further the hypothesis of a specific bonding interaction between the fluorine atom of the *R*-diastereomer and the guanidinium group of Arg183, we repeated the kinetic analysis with the separate (*R*)- and (*S*)-CHF diastereomers using a pol β mutant in which Arg183 was replaced with alanine (Fig. 5). No measurable difference was found between the catalytic insertion rate constants for the separate diastereomers ($k_{pol,R}$ = 0.27 s^{-1}; $k_{pol,S}$ = 0.29 s^{-1}), while there is a significant relative reduction in the apparent binding constant of the *S*-diastereomer ($K_{d,R}$ = 6.8 μM; $K_{d,S}$ = 39 μM) (Table 2). The overall stereospecificity favoring the incorporation of the *R*-diastereomer has been increased by about 1.5-fold for the mutant polymerase, stemming principally from a sizable (~ 6-fold) destabilization in binding of the *S*-isomer relative to that of the *R*-isomer, which may suggest a local repulsive effect.

For the Cl diastereomers, a specificity difference between the (*R*)-CHCl and (*S*)-CHCl diastereomers remains when R183 is replaced with Ala (Fig. 5B, Table 2). The difference between the *R* and *S* diastereomers in both the catalytic rate constant (~2x) and K_d (~3x) remains the same for both the wt and R183A mutant pol β (Table 2).

Discussion

In a recent review, Stahl *et al.*(23) usefully survey the phenomena of molecular interactions between ligands and receptors from the perspective of structure-based drug design, in which the medicinal chemist attempts to identify, inventory and optimize specific contributions of such interactions in the ground state to rationalize and enhance the overall binding affinity of, for example, an inhibitor for the enzyme site to which it binds. The authors emphasize the limitations and constraints imposed on attempts to map binding free energies to an analysis of three-dimensional structures, noting the difficulties encountered in correlating interactions observed in static ligand-protein complex structures with solution affinities.(23)

Nevertheless, it is well recognized that so-called weak hydrogen bonds between a covalently bound F atom in the ligand and a polar hydrogen atom HX (X = O, N) in the protein active site are frequently found in the PDB (23) and introduction of such interactions by design has been associated with increased ligand affinity.(23) Weak interactions of Cl and higher halogens with both electrophiles and nucleophiles have also been widely documented under the omnibus rubric of “halogen bonds” and in some instances can enhance binding of the halo-substituted ligand to a receptor site.(23) All the more challenging with respect to these considerations is the task of achieving a fundamental understanding of enzyme catalysis and specificity in terms of active site complex structures where multiple hydrophobic, electrostatic and steric interactions may contribute to an observed effect, and which requires the application of sophisticated transition state theory supported by powerful computational tools.(24, 25)

With these caveats in mind, we believe that our results allow several interesting conclusions. First, the precise placement of the CHX F or Cl atom in the active site of DNA pol β as determined by the choice of diastereomer can influence the energy of the transition state during turnover, particularly for the G•T mispair, as well as that of the ground state. Moreover, the fact that the diastereomers have congruent conformations in the pre-organized bound state suggests that these compounds represent a novel “testing bed” for *pairwise* comparisons of CHX interactions within the active site, because the strong electrostatic and other bonding of the “triphosphate” and sugar-base components largely predetermine the conformation of the nucleotide in the site, fixing the orientations in the two isomers of the C-X substituents and thereby creating a unique system to study weak interactions of the latter with the protein (which may also affect neighboring P-O oxygens).

Second, we previously synthesized a series of dNTP analogues having the β,γ-bridging oxygen replaced by a series of monohalo, dihalo, halo-methyl, azido-methyl, dimethyl and unsubstituted methylene groups.(17, 19, 26, 27) These compounds, comprising a “toolkit” currently with more than a dozen members, span a broad range of leaving group (bisphosphonic acid) pK_{a4} values: 7.8 (CF_2) to 12.3 (CMe_2). Owing to the widely different electronic and, in some instances, steric properties of the bisphosphonate moieties, the analogues are sensitive probes of deoxynucleotide incorporation and fidelity mechanisms for DNA polymerases (we are currently exploring the ability of the probes to act as substrates for other polymerases). In the case of pol β, analogues are incorporated by pol β in accord with a linear free energy relationship (LFER) between log k_{pol} vs. pK_{a4} that have negative slopes for dG vs. dC and dG vs. dT, thus affirming that the insertion (chemical) step (k_{pol}) is rate-limiting for both correct (W-C) and incorrect (non-W-C base pairs) catalysis.(15, 16, 28-31) In these experiments, the CXY analogues where $X \neq Y$ could only be tested as the diastereomer mixtures obtained by conventional synthetic procedures. For CHF and CHCl, the *R*:*S* ratio data now obtained for the individual diastereomers show that the mixed diastereomers’ averaged k_{pol} values are fair approximations with contributions from both isomers.

Third, we previously found that soaking DNA binary complex crystals of pol β with a 1:1 mixture of β,γ-CHF dGTP diastereomers resulted in a ternary complex with only (*R*)-β,γ-CHF dGTP observable. The estimated limit of detection for occupancy by the alternate stereoisomer suggested, approximately, a stereopreference of >3, i.e., (*S*)-β,γ-CHF might not be detected in the crystal if ≤ 25% present. In contrast, with β,γ-CHCl dGTP, both isomers detectably populated the active site. We have now shown by NMR analysis of the pol β-dependent reaction with the diastereomeric mixture that (*S*)-β,γ-CHF-dGTP is utilized with about 1/3 the efficiency of the *R*-diastereomer (Fig. 1). Kinetic results obtained with the separately synthesized diastereomers showed a 3.8-fold more efficient incorporation of (*R*)-β,γ-CHF-dGTP compared to the *S*-isomer (Table 1), in reasonable agreement with the indirect NMR measurements. Thus, the position of the fluorine atom must modulate the free energy of the transition state relative to the ground state.

Native pol β incorporates (*R*)-CHF with a 2-fold higher k_{pol} (Table 1). The structural data obtained with the *R*- and *S*-diastereomer mixture and with the separated *R*-diastereomer showed that the fluorine atom in the *R*-configuration is located 3.1 Å from a nitrogen atom of Arg183. The fluorine atom points away from Arg183 in the enzyme complex structure obtained with the separated *S*-diastereomer. The close proximity of the (*R*)-fluorine atom to Arg183 suggests that the discrimination in k_{pol} favoring *R* over *S* reflects a specific polar interaction between the fluorine atom and the guanidinium moiety of Arg183. Replacing Arg with Ala should eliminate any electrostatic interaction present, although it may replace it with a weak hydrophobic interaction, which is a known capability of the C-F group.(23) The kinetic data support a weak electrostatic interaction between the (*R*)-fluorine atom and the Arg183 because the R183A mutant pol β incorporates both *R*- and *S*-stereoisomers with almost identical values of k_{pol} (Table 2).

Next, the proximity of *R*-CHF with Arg183 prompts us to add new fuel to the longstanding and ongoing controversy over whether or not CF can form H-bonds.(32-35) Studies of organic halides (principally the C-F group) have suggested that these are very weak hydrogen bond acceptors.(23, 32, 36) Although a differentiation in terminology between hydrogen-bond formation and dipolar interaction might be viewed as being largely semantic, particularly since hydrogen bonding also has a dominant electrostatic component, there is clearly a conceptual issue stemming from the fact that hydrogen bonding also has a covalent component, whereas dipolar interactions by definition are purely electrostatic. In our study, the evidence for an electrostatic (dipolar) interaction between *R*-F and the guanidinium moiety is persuasive (Tables 1 and 2), however the 3.1 Å distance between *R*-F and Arg183 is clearly compatible with typical H-bonding distances.(37) Dalvit and Vulpetti(32, 36) have proposed an empirical correlation between the ^{19}F shifts and F-H interactions, in part using some of our own previously published data. (17, 18) Perhaps a computational analysis using an empirical valence bond treatment(38) could provide insight into whether or not an H-bond is formed. As mentioned above, since the nucleotide is held in place within the active site by strong charge interactions (“pre-organization”), the resulting complex offers an intriguing new system to evaluate the strength and origins of weak F-bonds in enzyme active sites.

Dalvit and Vulpetti have proposed a “Rule of Shielding” for drug design to utilize fluorinated moieties to enhance binding affinities, based on a proposed empirical correlation between the fluorine isotropic chemical shifts and their interactions with proteins observed in crystal structures.(32, 36) This empirical correlation suggested that shielded fluorines are found in close contact with hydrogen bond donors, whereas deshielded fluorines are often found to be near hydrophobic side chains or a backbone carbonyl, consistent with a dual character of fluorine as a potential hydrogen bond acceptor (or dipolar interaction partner), and as a hydrophobic group. Our CHF analogues exhibit a ^{19}F chemical shift of -216 ppm,

indicating strong shielding at the F atom, consistent with a disposition to act as a hydrogen bonding acceptor.

Despite the observed equal populations of the (*R*)- and (*S*)-β,γ-CHCl-dGTP in the tertiary crystal structure obtained with the diastereomer mixture, pol β incorporates the *R*-isomer 7-fold more efficiently than *S* (Fig. 3) and binds the *R*-isomer approximately three-fold better (Table 1). This "discrepancy" between the crystallography and the kinetic data cannot be explained simply by a detection limitation in the crystallography technique, and has been verified by both NMR and presteady state kinetic measurements (S = 6.3, Table 1). The stereospecificity is not caused solely by an interaction between the Cl atom of the *R*-isomer and the guanidinium group of R183, because there is still a significant difference between the k_{pol} values for the *S*- and *R*-isomers incorporated by the R183A mutant of pol β (Fig. 5, Table 2) (see below). A detailed explanation of the observed effects will require information about the structure of the transition state, differences between the crystal and solution complexes, and should account for any possible C-X interactions with nearby P-O oxygens.

The frequent occurrence of interactions between CF and polar H-atoms has been mentioned. The other halogens (Cl, Br and I) sometimes have significant interactions with carbonyl groups or other classical H-bond acceptors, that are collectively referred to as "halogen bonds".(23) Such interactions have been verified by structural and structure-activity relationship (SAR) data.(23) Although halogen bonds formed by chlorine are typically weak, they can play a unique role in some complexes, i.e. triclosan, a broad spectrum bactericide containing a chlorine atom interacting at a distance of 3.3 – 3.5 Å with a backbone carbonyl in the FabI active site. Replacement of the chlorine atom with lipophilic or hydrogen bonding substituents did not lead to compounds with higher potency.(23)

Regardless of their details, the evidence provided by our kinetics studies for the importance of CHX stereochemistry in β,γ-CXY dGTP substrates of pol β under dynamic, turnover conditions gives further support for an intriguing translational opportunity. Pol β has generated considerable interest as a target for the development of inhibitors based on its overriding importance in single-nucleotide BER(1, 2) and its implied role in cancer.(3-12) Arg183 in pol β could be a unique active site target for selective inhibition based on its unique role in family X DNA polymerases.

Supplementary Material

Refer to Web version on PubMed Central for supplementary material.

Abbreviations

pol DNA polymerase

References

1. Matsumoto Y, Kim K. Excision of deoxyribose phosphate residues by DNA polymerase beta during DNA repair. Science. 1995; 269:699–702. [PubMed: 7624801]
2. Piersen CE, Prasad R, Wilson SH, Lloyd RS. Evidence for an imino intermediate in the DNA polymerase beta deoxyribose phosphate excision reaction. J Biol Chem. 1996; 271:17811–17815. [PubMed: 8663612]
3. Srivastava DK, Husain I, Arteaga CL, Wilson SH. DNA polymerase beta expression differences in selected human tumors and cell lines. Carcinogenesis. 1999; 20:1049–1054. [PubMed: 10357787]

4. Bhattacharyya N, Chen HC, Comhair S, Erzurum SC, Banerjee S. Variant forms of DNA polymerase beta in primary lung carcinomas. DNA Cell Biol. 1999; 18:549–554. [PubMed: 10433553]
5. Bhattacharyya N, Chen HC, Grundfest-Broniatowski S, Banerjee S. Alteration of hMSH2 and DNA polymerase beta genes in breast carcinomas and fibroadenomas. Biochem Biophys Res Commun. 1999; 259:429–435. [PubMed: 10362525]
6. Dobashi Y, Shuin T, Tsuruga H, Uemura H, Torigoe S, Kubota Y. DNA polymerase beta gene mutation in human prostate cancer. Cancer Res. 1994; 54:2827–2829. [PubMed: 8187060]
7. Dong Z, Zhao G, Zhao Q, Yang H, Xue L, Tan X, Zheng N. A study of DNA polymerase beta mutation in human esophageal cancer. Zhonghua Yi Xue Za Zhi. 2002; 82:899–902. [PubMed: 12126515]
8. Iwanaga A, Ouchida M, Miyazaki K, Hori K, Mukai T. Functional mutation of DNA polymerase beta found in human gastric cancer--inability of the base excision repair in vitro. Mutat Res. 1999; 435:121–128. [PubMed: 10556592]
9. Matsuzaki J, Dobashi Y, Miyamoto H, Ikeda I, Fujinami K, Shuin T, Kubota Y. DNA polymerase beta gene mutations in human bladder cancer. Mol Carcinog. 1996; 15:38–43. [PubMed: 8561864]
10. Miyamoto H, Miyagi Y, Ishikawa T, Ichikawa Y, Hosaka M, Kubota Y. DNA polymerase beta gene mutation in human breast cancer. Int J Cancer. 1999; 83:708–709. [PubMed: 10521812]
11. Starcevic D, Dalal S, Sweasy JB. Is there a link between DNA polymerase beta and cancer? Cell Cycle. 2004; 3:998–1001. [PubMed: 15280658]
12. Wang L, Patel U, Ghosh L, Banerjee S. DNA polymerase beta mutations in human colorectal cancer. Cancer Res. 1992; 52:4824–4827. [PubMed: 1511447]
13. Horton JK, Wilson SH. Hypersensitivity phenotypes associated with genetic and synthetic inhibitor-induced base excision repair deficiency. DNA Repair. 2007; 6:530–543. [PubMed: 17113833]
14. Madhusudan S, Middleton MR. The emerging role of DNA repair proteins as predictive, prognostic and therapeutic targets in cancer. Cancer treatment reviews. 2005; 31:603–617. [PubMed: 16298073]
15. Sucato CA, Upton TG, Kashemirov BA, Batra VK, Martinek V, Xiang Y, Beard WA, Pedersen LC, Wilson SH, McKenna CE, Florian J, Warshel A, Goodman MF. Modifying the beta,gamma leaving-group bridging oxygen alters nucleotide incorporation efficiency, fidelity, and the catalytic mechanism of DNA polymerase beta. Biochemistry. 2007; 46:461–471. [PubMed: 17209556]
16. Sucato CA, Upton TG, Kashemirov BA, Osuna J, Oertell K, Beard WA, Wilson SH, Florian J, Warshel A, McKenna CE, Goodman MF. DNA polymerase beta fidelity: halomethylene-modified leaving groups in pre-steady-state kinetic analysis reveal differences at the chemical transition state. Biochemistry. 2008; 47:870–879. [PubMed: 18161950]
17. Batra VK, Pedersen L, Beard WA, Wilson SH, Kashemirov BA, Upton T, Goodman MF, McKenna CE. Halogenated β,γ-methylene- and ethylidene-dGTP-DNA ternary complexes with DNA polymerase β: structural evidence for stereospecific binding of the fluoromethylene analogues. J. Am. Chem. Soc. 2010; 132:7617–7625. [PubMed: 20465217]
18. McKenna CE, Kashemirov BA, Upton T, Batra VK, Goodman MF, Pedersen L, Beard WA, Wilson SH. (R)-β,γ-fluoromethylene-dGTP-DNA ternary complex with DNA polymerase β. J Am Chem Soc. 2007; 129:15412–15413. [PubMed: 18031037]
19. Wu Y, Zakharova VM, Kashemirov BA, Goodman MF, Batra VK, Wilson SH, McKenna CE. β,γ-CHF- and β,γ-CHCl-dGTP Diastereomers: Synthesis, Discrete 31P NMR Signatures, and Absolute Configurations of New Stereochemical Probes for DNA Polymerases. J Am Chem Soc. 2012; 134:8734–8737. [PubMed: 22397499]
20. Beard WA, Wilson SH. Purification and domain-mapping of mammalian DNA polymerase beta. Methods Enzymol. 1995; 262:98–107. [PubMed: 8594388]
21. Bertram JG, Oertell K, Petruska J, Goodman MF. DNA polymerase fidelity: comparing direct competition of right and wrong dNTP substrates with steady state and pre-steady state kinetics. Biochemistry. 2010; 49:20–28. [PubMed: 20000359]
22. Fersht, AR. Enzyme Structure and Mechanism. 2 ed.. W.H. Freeman & Co.; New York: 1985.

23. Bissantz C, Kuhn B, Stahl M. A Medicinal Chemist's Guide to Molecular Interactions. J Med Chem. 2010; 53:5061–5084. [PubMed: 20345171]
24. Braun-Sand SO, Mats HM, Warshel A. Computer Modeling of Enzyme Catalysis and its Relationship to Concepts in Physical Organic Chemistry. 2005; 40
25. Lu Y, Wang Y, Zhu W. Nonbonding interactions of organic halogens in biological systems: implications for drug discovery and biomolecular design. Phys Chem Chem Phys. 2010; 12:4543–4551. [PubMed: 20428531]
26. Chamberlain BT, Upton TG, Kashemirov BA, McKenna CE. α-Azido bisphosphonates: synthesis and nucleotide analogues. J Org Chem. 2011; 76:5132–5136. [PubMed: 21462930]
27. Chamberlain BT, Batra VK, Beard WA, Kadina AP, Shock DD, Kashemirov BA, McKenna CE, Goodman MF, Wilson SH. Stereospecific Formation of a Ternary Complex of (S)-α,β-Fluoromethylene-dATP with DNA Pol β. ChemBioChem. 2012; 13:528–530. [PubMed: 22315190]
28. Bakhtina M, Roettger MP, Tsai MD. Contribution of the reverse rate of the conformational step to polymerase beta fidelity. Biochemistry. 2009; 48:3197–3208. [PubMed: 19231836]
29. Lin P, Batra VK, Pedersen LC, Beard WA, Wilson SH, Pedersen LG. Incorrect nucleotide insertion at the active site of a G:A mismatch catalyzed by DNA polymerase beta. Proc Natl Acad Sci U S A. 2008; 105:5670–5674. [PubMed: 18391201]
30. Lin P, Pedersen LC, Batra VK, Beard WA, Wilson SH, Pedersen LG. Energy analysis of chemistry for correct insertion by DNA polymerase beta. Proc Natl Acad Sci U S A. 2006; 103:13294–13299. [PubMed: 16938895]
31. Tsai YC, Johnson KA. A new paradigm for DNA polymerase specificity. Biochemistry. 2006; 45:9675–9687. [PubMed: 16893169]
32. Dalvit C, Vulpetti A. Fluorine-protein interactions and (1)F NMR isotropic chemical shifts: An empirical correlation with implications for drug design. ChemMedChem. 2011; 6:104–114. [PubMed: 21117131]
33. Liu D, Moran S, Kool ET. Bi-stranded, multisite replication of a base pair between difluorotoluene and adenine: confirmation by ‘inverse’ sequencing. Chem Biol. 1997; 4:919–926. [PubMed: 9427657]
34. Lu Y, Wang Y, Xu Z, Yan X, Luo X, Jiang H, Zhu W. C-X...H contacts in biomolecular systems: how they contribute to protein-ligand binding affinity. J Phys Chem B. 2009; 113:12615–12621. [PubMed: 19708644]
35. Moran S, Ren RX, Rumney S, Kool ET. Difluorotoluene, a Nonpolar Isostere for Thymine, Codes Specifically and Efficiently for Adenine in DNA Replication. J Am Chem Soc. 1997; 119:2056–2057. [PubMed: 20737028]
36. Dalvit C, Vulpetti A. Intermolecular and Intramolecular Hydrogen Bonds Involving Fluorine Atoms: Implications for Recognition, Selectivity, and Chemical Properties. ChemMedChem. 2012; 7:262–272. [PubMed: 22262517]
37. Wallwork SC. Hydrogen-Bond Radii. Acta Cryst. 1962; 15:758–759.
38. Aaqvist J, Warshel A. Simulation of enzyme reactions using valence bond force fields and other hybrid quantum/classical approaches. Chemical Reviews. 1993; 93:2523–2544.

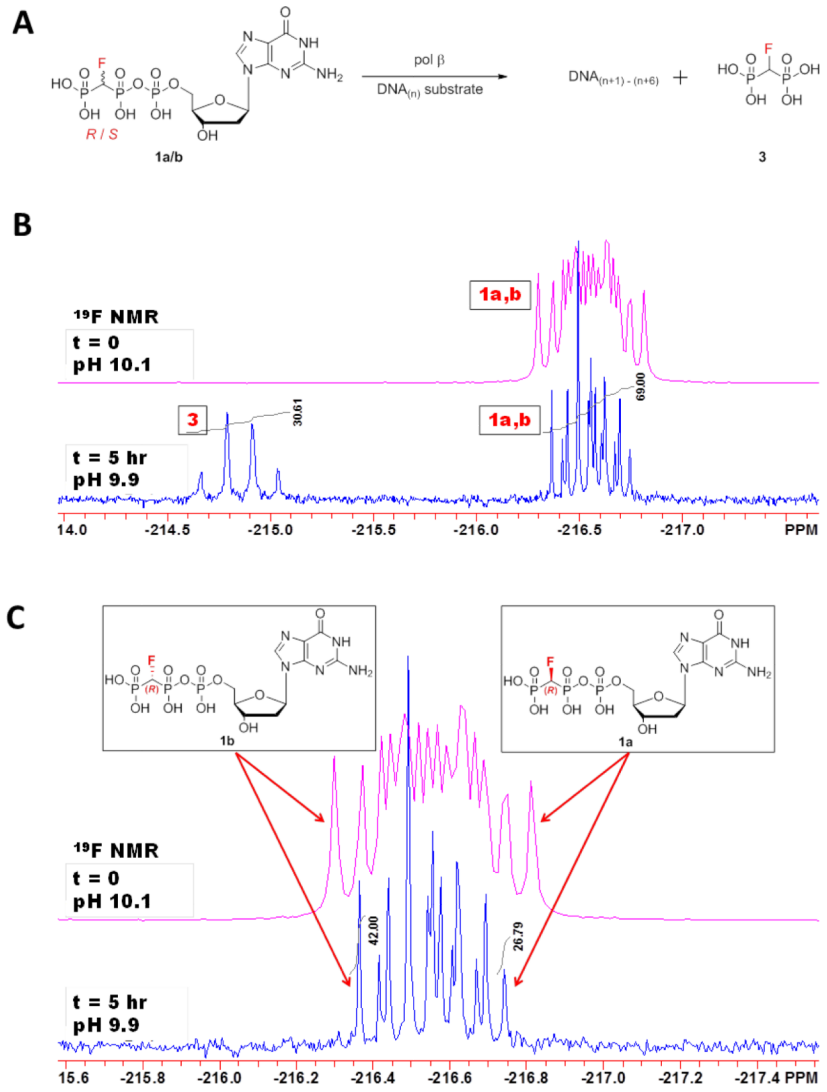

Figure 1.

Reaction scheme and ^{19}F NMR spectra of reaction mixtures. (A) Sketch depicting the direct competition reaction carried out for the NMR analysis. β,γ-CHF-dGTP andp-CHF-p bisphosphonate are labeled below for identification with NMR spectra. $DNA_{(n+1)-(n+6)}$ denotes that up to 6 correct nt can be inserted opposite the 6 consecutive dCs in the template (see Materials and Methods). (B) β,γ-CHF-dGTP in an equal mixture of *R* and *S* is incubated with primer/template DNA with wt pol β, and ^{19}F NMR spectra are taken at time zero (upper pink trace) and after a five hour incubation (lower blue trace). Peaks are labeled as in A. (C) Zoom in of peaks corresponding to unreacted β,γ-CHF-dGTP analogue (1a and 1b) at time zero (upper pink trace) and after five hours (lower blue trace). The outer peaks can be used to specifically identify and quantitate the individual diastereomers, with the downfield (left) peak corresponding to the *S* diastereomer (1b), and the upfield (right) peak corresponding to the *R* (1a). dGMP (**2**) from hydrolysis was < 2% by ^{31}P NMR (Figure S1 of the Supporting Information).

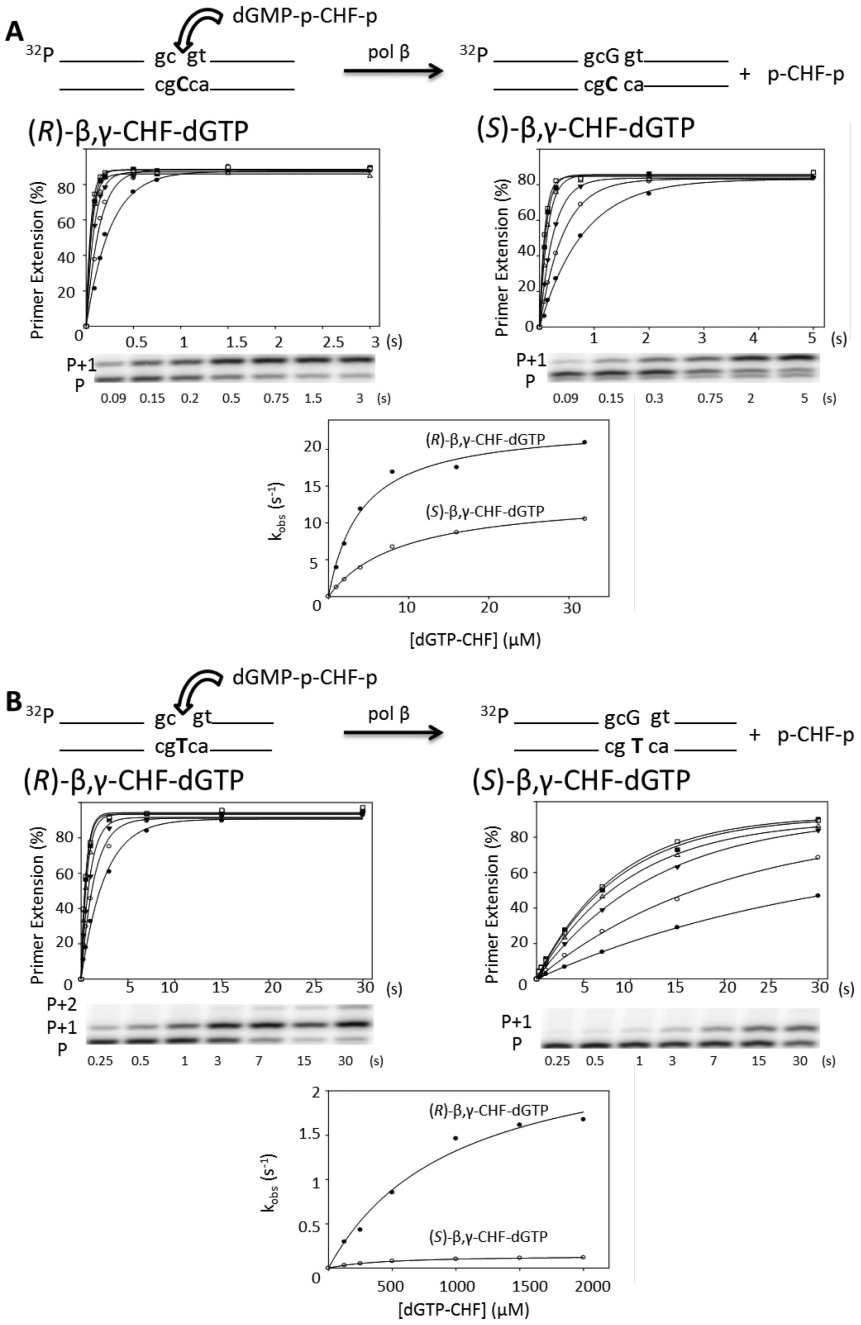

Figure 2.

Presteady state incorporation into single-gap DNA substrate reactions with separate CHF diastereomers. (A) Correct incorporation opposite dC of *R* (left) and *S* (right) diastereomers. The plot of percentage primer extension vs. time is shown for all six concentrations of analogue (1 μM, filled circles; 2 μM, open circles; 4 μM, filled triangles; 8 μM, open triangles; 16 μM, filled squares; 32 μM, open squares), below which is a representative gel showing a time course with 1 μM analogue. The corresponding reaction time is shown below each lane. P represents the unextended primer, and P+1 the extension by a single dGMP. The observed rate constant is plotted opposite the corresponding analogue concentration for both the *R* and *S* analogues on the same plot for comparison purposes. (B) Misincorporation opposite dT of *R* (left) and *S* (right) diastereomers. The plot of percentage

primer extension vs. time is shown for all six concentrations of analogue (125 μM, filled circles; 250 μM, open circles; 500 μM, filled triangles; 1000 μM, open triangles; 1500 μM, filled squares; 2000 μM, open squares), below which is a representative gel showing a time course with 125 μM analogue. P represents the unextended primer, P+1 the extension by a single dGMP, and P+2 a second incorporation by displacement of the downstream oligonucleotide, which is only observed for the *R* diastereomer. The corresponding reaction time is shown below each lane. The observed rate constant is plotted opposite the corresponding analogue concentration for both the *R* and *S* analogues on the same plot for comparison purposes. The reactions were carried out in triplicate and have an SEM of ± 15%; the figure shows a representative data set.

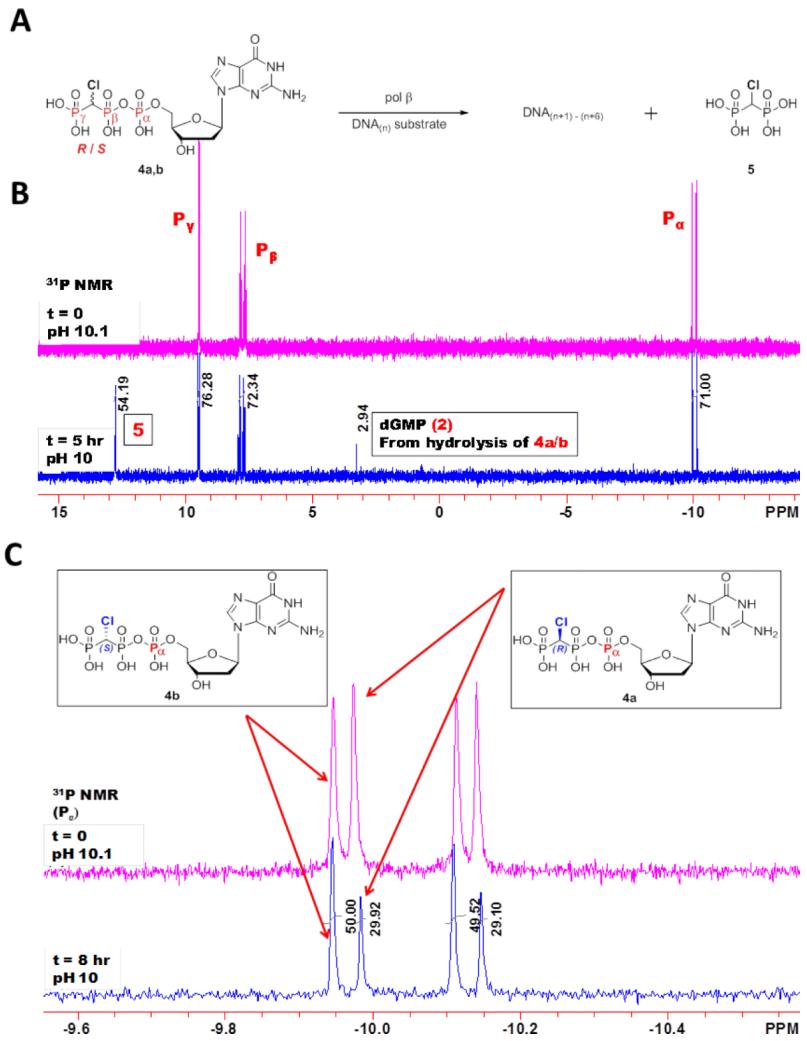

Figure 3.

Reaction scheme and ^{31}P NMR spectra of (*R/S*)-β,γ-CHCl-dGTP reaction mixtures. (A) Reaction scheme depicting the direct competition between (*R*)-β,γ-CHCl-dGTP and (*S*)-β,γ-CHCl-dGTP for incorporation into DNA by wild type pol β. Phosphorus atoms of (*R/S*)-β,γ-CHCl-dGTP and p-CHCl-p bisphosphonate are labeled for reference in the NMR spectra. $DNA_{(n+1)-(n+6)}$ denotes that up to 6 correct nt can be inserted opposite the 6 consecutive dCs in the template (see Materials and Methods). (B) Primer/template DNA is incubated with wt pol β and (*R/S*)-β,γ-CHCl-dGTP in a 50:50 mixture of *R*:*S*. ^{31}P NMR spectra are taken at time zero (upper pink trace), and after 8 hours incubation at 37°C (lower blue trace) following treatment as described in Methods. Peaks are labeled as in A. (C) Zoom in of the region of interest around the P_α. Leftmost peak is due to (*S*)-β,γ-CHCl-dGTP (4b) alone, while the peak at ~ -10 ppm) is due to (*R*)-β,γ-CHCl-dGTP (4a) alone.

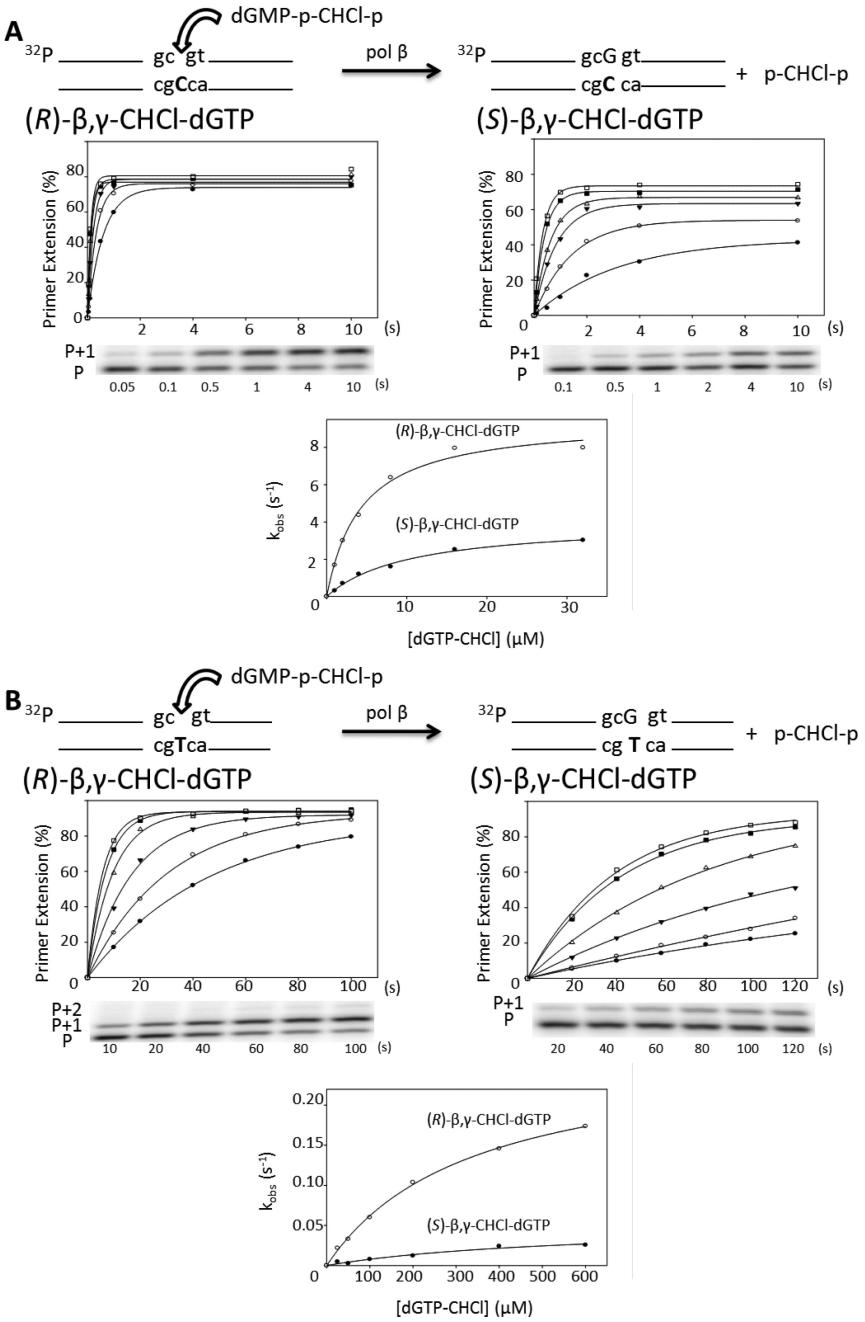

Figure 4.

Presteady state incorporation of (R/S)-β,γ-CHCl-dGTP into single-gapped DNA. (A) Correct incorporation opposite dC of *R* (left) and *S* (right) CHCl diastereomers. The cartoon shows the generalized scheme for the reaction. A plot of the percentage of primer extension vs. time for six concentrations of the CHCl analogue is shown for one of three repeats of each reaction (1 μM, filled circles; 2 μM, open circles; 4 μM, filled triangles; 8 μM, open triangles; 16 μM, filled squares; 32 μM, open squares). Below each plot is a time course shown on a representative gel for the first concentration (1 μM), where P represents the unextended primer and P+1 the extension of the primer by a single incorporation. The corresponding reaction time is shown below each lane. Below these gels is a plot of the observed rate constant vs. the corresponding analogue concentration for both diastereomers.

(B) Misincorporation opposite dT of *R* (left) and *S* (right) CHCl diastereomers. As for the correct pairing, the percentage of primer extension vs. time for each concentration of analogue is shown for both diastereomers (25 μM, filled circles; 50 μM, open circles; 100 μM, filled triangles; 200 μM, open triangles; 400 μM, filled squares; 600 μM, open squares) with a representative gel for each set of reactions; the corresponding reaction time is shown below each lane. The observed rate constant is plotted vs. the corresponding analogue concentration on the same plot for each diastereomer below. The reactions were carried out in triplicate and have an SEM of ± 15%; the figure shows a representative data set.

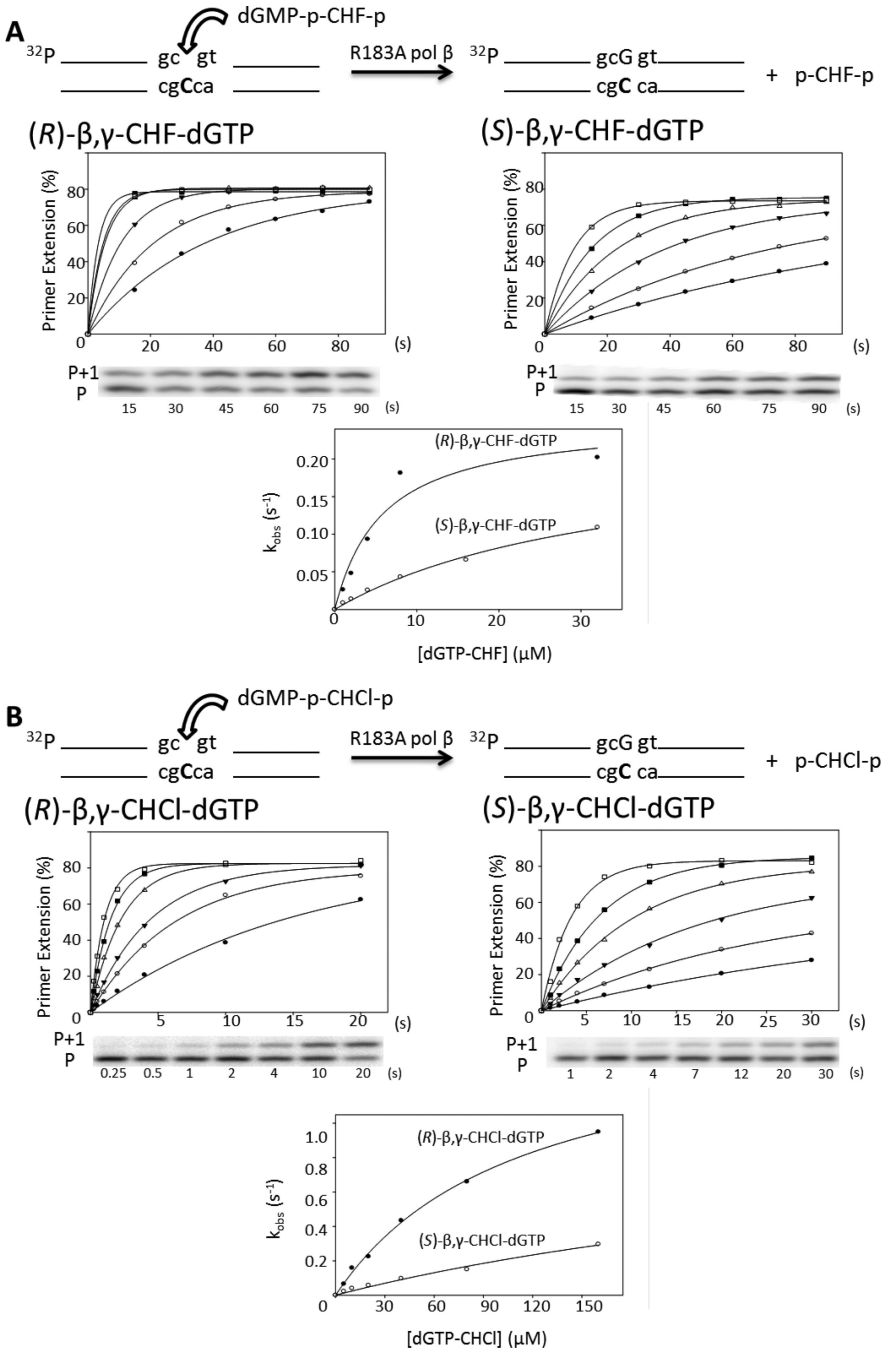

Figure 5.

Presteady state incorporation by R183A pol β into single-gap DNA substrate reactions with separate diastereomers. (**A**) Correct incorporation opposite dC of (*R*)-β,γ-CHF-dGTP (left) and (*S*)-β,γ-CHF-dGTP (right) diastereomers. The plot of percentage primer extension vs. time is shown for all six concentrations of analogue (1 μM, filled circles; 2 μM, open circles; 4 μM, filled triangles; 8 μM, open triangles; 16 μM, filled squares; 32 μM, open squares), below which is a representative gel showing a time course with 1 μM analogue. P represents the unextended primer, and P+1 the extension by a single dGMP. The corresponding reaction time is shown below each lane. The observed rate constant is plotted opposite the corresponding analogue concentration for both the *R* and *S* analogues on the

same plot for comparison purposes. (**B**) Correct incorporation opposite dC of (R)-β,γ-CHCl-dGTP (left) and (*S*)-β,γ-CHCl-dGTP (right) by R183A pol β. The plot of percentage primer extension vs. time is shown for each concentration of analogue (5 μM, filled circles; 10 μM, open circles; 20 μM, filled triangles; 40 μM, open triangles; 80 μM, filled squares; 160 μM, open squares) with a representative gel picture underneath; the corresponding reaction time is shown below each lane. The observed rate constant is plotted vs. the corresponding analogue concentration below. The reactions were carried out in triplicate and have an SEM of ± 15%; the figure shows a representative data set.

Table 1

Presteady state parameters for correct and incorrect incorporation of *R* and *S* CHF and CHCl diastereomers by wt pol β. k_{pol}, K_d and stereospecificity values are reported as the mean ± standard error of three replicates. Stereospecificity is defined as $(k_{pol}/K_d)_R/(k_{pol}/K_d)_S$.

Pairing	Diastereomer	k_{pol} (s^{-1})	K_d (μM)	Stereospecificity
Opposite C	(*R*)-CHF	18 ± 3	6.2 ± 2.2	3.8 ± 0.4
	(*S*)-CHF	9.2 ± 2.3	10 ± 1	
	(*R*)-CHCl	7.6 ± 1.2	3.2 ± 0.8	6.3 ± 0.8
	(*S*)-CHCl	4.8 ± 0.4	11 ± 1	
Opposite T	(*R*)-CHF	2.3 ± 0.4	740 ± 140	11 ± 1
	(*S*)-CHF	0.16 ± 0.01	590 ± 110	
	(*R*)-CHCl	0.26 ± 0.01	290 ± 20	7.8 ± 0.4
	(*S*)-CHCl	0.051 ± 0.003	540 ± 30	

Table 2

Presteady state parameters for correct incorporation of *R* and *S* CHF and CHCl diastereomers by R183A pol β. k_{pol} and K_d values are reported as the mean ± standard error of three replicates.

Diastereomer	k_{pol} (s^{-1})	K_d (μM)
(*R*)-CHF	0.27 ± 0.02	6.8 ± 1.0
(*S*)-CHF	0.29 ± 0.06	39 ± 8
(*R*)-CHCl	1.5 ± 0.1	110 ± 3
(*S*)-CHCl	0.88 ± 0.13	300 ± 96